Sustainable Energy & Fuels

X-ray absorption spectroscopy of Ba- and Cs-promoted Ru/Mesoporous carbon catalysts for long-term ammonia synthesis under intermittently varied conditions

Journal:	*Sustainable Energy & Fuels*
Manuscript ID	SE-ART-09-2019-000781.R1
Article Type:	Paper
Date Submitted by the Author:	24-Oct-2019
Complete List of Authors:	Nishi, Masayasu; National Institute of Advanced Industrial Science and Technology, Research Institute of Energy Frontier Chen, Shih-Yuan; National Institute of Advanced Industrial Science and Technology (AIST), Energy Catalyst Technology Group, Research Institute of Energy Frontier Takagi, Hideyuki; National Institute of Advanced Industrial Science and Technology (AIST)

ARTICLE

X-ray absorption spectroscopy of Ba- and Cs-promoted Ru/Mesoporous carbon catalysts for long-term ammonia synthesis under intermittently varied conditions

Received 00th January 20xx,
Accepted 00th January 20xx

DOI: 10.1039/x0xx00000x

Masayasu Nishi,*[a] Shih-Yuan Chen [a] and Hideyuki Takagi [a]

The structural characters of Ba- and Cs-promoted Ru catalysts supported on a mesoporous carbon material were examined by X-ray absorption spectroscopy and several characterization techniques, and correlated to their activities in long-term ammonia synthesis under intermittently varied conditions. The 0.5Ba-10 wt.%Ru/MPC contains barium species adhered to the surfaces of the Ru nanoparticles, creating more catalytically active sites for the dissociation of nitrogen molecules. By contrast, the 2.5Cs-10 wt.%Ru/MPC contains cesium hydroxides homogeneously covered on the MPC and Ru interfaces, enhancing the electronic property of the Ru nanoparticles and consequently facilitating ammonia synthesis. Therefore, the ammonia synthesis rates over these promoted Ru catalyst could be finely and stably tuned within 22.5–100 mmol g_{cat}^{-1} h^{-1} by quickly varying the reaction temperatures of 340–400 °C and gas hourly space velocity of 9,000–18,000 h^{-1}, which intermittently varied conditions could meet with hydrogen production rates derived from sustainable process.

1. Introduction

During the past few decades, the human population has rapidly grown to approximately 7.5 billion, accelerating the conversion of fossil fuels, such as coal, petroleum, and natural gas, to meet the world's energy demand.[1] However, CO_2, a byproduct of fossil fuel burning, has been largely released into the atmosphere, causing serious environmental problems, particularly global warming, an increase in extreme climate change, and ocean acidification. The Japan meteorological agency has recorded a high concentration of CO_2 (~410 ppm) near Okinawa prefecture,[2] which is approaching to the upper limit of atmospheric CO_2 concentration required to suppress the increase in global temperature to less than 1.5–2 °C, which is the goal of with the COP21 led Paris Agreement.[3] To adhere to the Paris Agreement, the Japanese government has legislated a national energy policy on the reduction of CO_2 emissions by 80% by 2050, in comparison to the values achieved in 2013. To achieve this forward-looking goal, Japan has focused on the development of new energy systems and their infrastructure, particularly it has generated a hydrogen society using hydrogen as a clean fuel with low CO_2 emissions by burning, instead of using conventional fossil energy sources. However, hydrogen is difficult to liquefy (< –253 °C), easily flammable, and expensive. The construction of hydrogen stations and the related infrastructure for hydrogen production, storage, transport, and utilization as a fuel source remain a challenge.

Hydrogen carriers can be a possible solution to accelerating the transformation of the current modern society into a new hydrogen society, in which hydrogen is converted into candidate molecules with suitable properties, such as ammonia, methylbenzene, and formic acid, allowing the technical problems described above to be resolved. Among the different types of hydrogen carriers, ammonia is a potential molecule that has been widely used in the fertilizer industry. Ammonia, containing approximately 17 wt.% hydrogen, can be easily liquified at –33 °C under ambient conditions. In addition, the ammonia industry has a well-constructed infrastructure, which can be immediately applied to a new hydrogen carrier industry. Recent reports have further demonstrated that ammonia can be burned as a fuel through a co-feeding process using natural gas or coal to generate electricity, thereby reducing CO_2 emissions.[4] However, ammonia is conventionally synthesized through the chemical reactions of nitrogen and hydrogen catalyzed by a modified Fe_3O_4-K_2O-Al_2O_3 catalyst under severe conditions (400–600 °C, 20–40 MPa), which is the so-called Haber-Bosch process developed by Haber and Bosch nearly a century ago.[5] In ammonia synthesis, hydrogen is mostly obtained through the steam reforming of methane coupled with a water-gas shift reaction, which consumes a large amount of energy globally (~1–2%) and consequently releases large amounts of CO_2. Recent studies have attempted to develop new catalytic processes or innovative materials that are able to achieve a sustainable ammonia synthesis under mild conditions with low CO_2 emissions.[6] Pioneering studies have demonstrated that ammonia can be sustainably synthesized through the conversion of nitrogen and hydrogen over promoted Ru-based catalyst under mild reaction conditions.[7,8] Advanced studies have further demonstrated next-generation Ru-based catalysts with enhanced activity and durability for an energy-effective production of ammonia at relatively low temperature and pressure.[9–18] Our previous studies indicated that hydrogen with a low carbon footprint can be used as

[a] *Energy Catalyst Technology Group, Research Institute of Energy Frontier (RIEF), Department of Energy and Environment, National Institute of Advanced Industrial Science and Technology (AIST), 16-1 Onogawa, Tsukuba, Ibaraki 305-8589, Japan.* E-mail: m.nishi@aist.go.jp

†Electronic Supplementary Information (ESI) available: See DOI: 10.1039/x0xx00000x

a feedstock for mild ammonia synthesis over alkali- and alkaline-earth-promoted Ru-based catalysts, although its production cost must be reduced for future commercialization.[19–21] It should be noted that the production rate of hydrogen with a low carbon footprint through the electrolysis of water is variable and significantly dependent of the nature of the intermittent energy source, such as solar cell power stations, wind power generation, and hydroelectric power. In other words, alkali- and alkaline-earth-promoted Ru-based catalysts must achieve a high performance, good durability, and quick responsibility to meet the large variation in the production of hydrogen with a low carbon footprint when used as a feedstock for a mild ammonia synthesis, which have yet to be fully discussed. Herein, ammonia synthesis over alkali- and alkaline-earth-promoted Ru-based catalysts, i.e., Cs-Ru/MPC and Ba-Ru/MPC, was studied using a fixed-bed reactor under intermittently varied conditions under a wide range of GHSV and temperature for more than 50 h and eight run cycles. The influence of porosities and promotors on the catalytic performance and active sites of prepared Cs-Ru and Ba-Ru catalysts were surveyed at the molecular scale using X-ray absorption spectroscopy, the results of which were combined with the findings of conventional characterizations of powdered X-ray diffraction (PXRD), N_2 and CO sorption, and electronic microscopy.

2. Experimental

2.1 Preparation of Cs- and Ba-promoted Ru/MPC and Ru/AC catalysts

A commercial mesoporous carbon material with an annealing temperature of 1,800 °C (denoted as MPC; product code, CNovel®P(3)010) was kindly supplied by Toyo Tanso Co. Ltd., Japan. Activated carbon (AC) with a microporous structure (product code, HG15-119, produced by Osaka Gas Chemical Co., Ltd., Japan) was thermally treated at 500 °C in a H_2 flow for 3 h before use. Ruthenium(III) nitrosyl nitrate ($Ru(NO)(NO_3)_3$) (Ru content = 31.7 wt.%, Mitsuwa Chemicals Co., Ltd., Japan) as a Ru precursor was used as received. Barium nitrate ($Ba(NO_3)_2$) (Wako Co. Ltd.,) and cesium carbonate (Cs_2CO_3) (Alfa Aesar) were used as Ba and Cs promoters, respectively. Through a typical synthesis, 1 g of MPC or AC was dispersed in an ethanol-water solution (50%, v/v) containing 0.31 g of $Ru(NO)(NO_3)_3$. The Ru-impregnated MPC and AC samples (denoted as 10Ru/MPC and 10Ru/AC, respectively) were obtained by evaporating the solvent at 70 °C under stirring, followed by calcining at 400 °C in N_2 for 3 h. The Ru loading was optimized at 10 wt.% based on the weight of carbon [20]. For the impregnation of the promoter (Cs or Ba), 0.13 g of $Ba(NO_3)_2$ or 0.41 g of Cs_2CO_3 was impregnated onto the 10Ru/MPC and 10Ru/AC samples using procedures without a calcination step as previously mentioned. The Ba loadings were varied within the range of 1.2–5.5 wt.%, corresponding to Ba/Ru molar ratios of 0.1–0.5. The Cs loadings were varied within the range of 1.2–22 wt.%, corresponding to Cs/Ru molar ratios of 0.1–2.5. The resultant samples were denoted as xCs-10Ru/MPC, yBa-10MPC, xCs-10Ru/AC, and yBa-10Ru/AC, where x and y represent the Cs/Ru and Ba/Ru molar ratios, respectively.

2.2 Characterizations

The PXRD patterns were recorded using a MiniFlex600 diffractometer (Rigaku Ltd., Japan) using a Cu *K*α radiation (λ = 0.154184 nm) operated at 40 kV and 15 mA. Nitrogen adsorption–desorption isotherms were measured using a BELSORP-max instrument (MicrotracBEL Corp., Japan) at 77 K. For the MPC-series samples, the structural properties, such as the specific surface area and pore volume, were determined using the Brunauer–Emmet–Taylor (BET) method and a Dubinin–Astakhov (DA) analysis,[22] respectively. For the AC-series samples, the subtracting pore effect (SPE) method[23] was used for the high-resolution α_s-plot. The Ru particle size and size distribution were analyzed by high-resolution transmission electron microscopy (HRTEM) using a TOPCON EM002B instrument at an accelerating voltage of 120 kV. The Ru particle size and dispersion were also determined by a CO chemisorption technique using an Ohkura Riken R6015 instrument by assuming a stoichiometric CO/Ru ratio of 1. Before the CO chemisorption, the samples were reduced at 450 °C for 2 h in a hydrogen flow of 50 mL min^{-1}, followed by purging with a helium flow of 50 mL min^{-1} until the TCD signal was stable at 50 °C. For the CO chemisorption, a sequence of 10%CO/He pulse was injected to the pre-treated samples at 50 °C until more CO molecules were observed. In addition, Ru, Cs, and Ba *K*-edge X-ray absorption spectra recorded within the energy regions of 21.614–23.219, 35.472–37.105, and 36.932–38.581 keV, respectively, were obtained at the National Laboratory for High Energy Accelerator Research Organization (KEK), Tsukuba, Japan. The NW-10A beamline of PF-AR at KEK was operated at 6.5 GeV and 60 mA. The synchrotron X-ray was monochromatized using a Si(311) double-crystal monochromator and calibrated through a self-supported Ru^0 pellet. Before the measurement, the catalysts and boron nitride were homogeneously mixed into self-supported pallets, where the catalyst weights in the final mixtures were approximately 60–70 wt.%. The XANES and EXAFS spectra were fitted using the IFEFFIT code through the FEFF6 procedure.[24, 25]

2.3 Mild ammonia synthesis

The mild ammonia synthesis over the prepared Ba-Ru or Cs-Ru catalysts was examined using a fixed-bed reactor with a quartz inlet in which the catalyst bed with a volume of 0.8 mL was finely sandwiched by a quartz wool under a typical reaction condition, and then further studied using the same reactor under intermittently varied conditions. The prepared catalysts were reduced at 450 °C under a H_2 flow (GHSV = 10,000 h^{-1}) for 2 h prior to the ammonia synthesis. Under typical reaction conditions, a mild ammonia synthesis over the prepared Ba-Ru and Cs-Ru catalysts was conducted within a reaction temperature range of 280–550 °C and a pressurized atmosphere of 0.99 MPa. A mixed gas of H_2 and N_2 (H_2/N_2 ratio = 3) with a flow rate of 120 mL min^{-1} was applied, corresponding to a GHSV value of 9,000 h^{-1}. For the mild ammonia synthesis

under intermittently varied conditions, the reaction temperatures were quickly varied with a time interval of 3 h

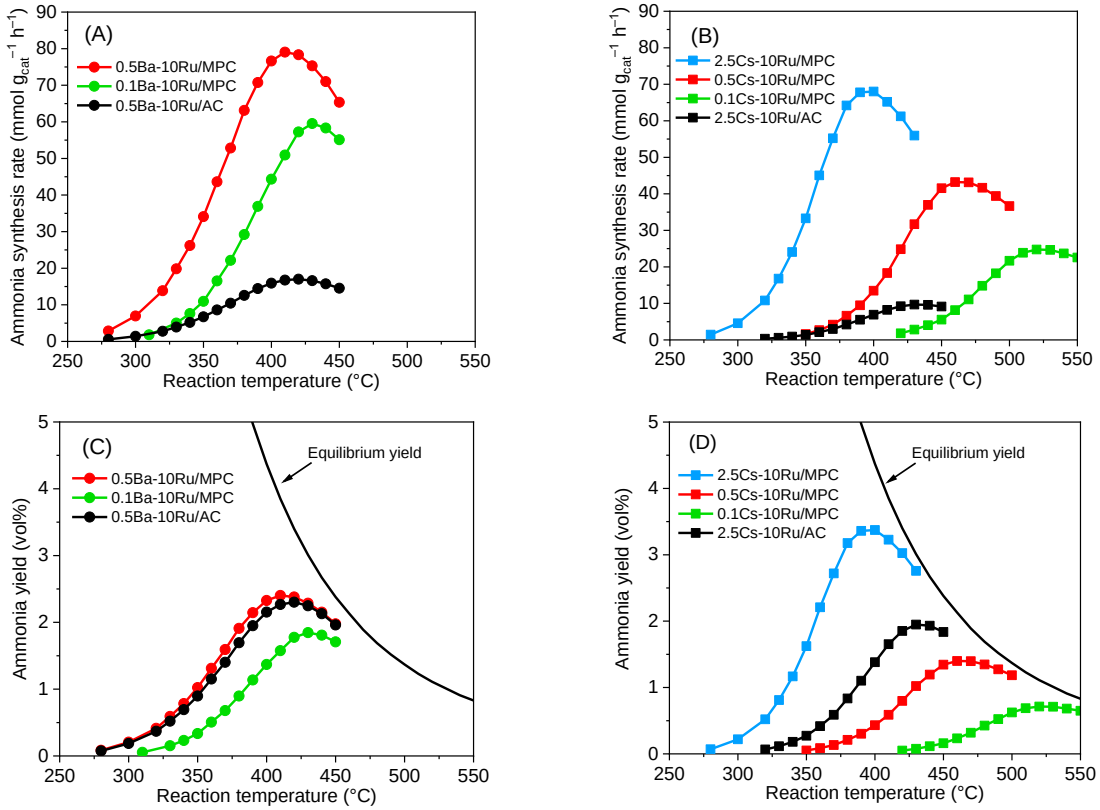

Fig. 1 Temperature dependence of ammonia synthesis rate and yield over (A, C) yBa-10Ru/AC and yBa-10Ru/MPC catalysts and (B, D) xCs-10Ru/AC and xCs-10Ru/MPC catalysts at 0.99 MPa, H_2/N_2 = 3, GHSV = 9,000 h^{-1}.

within a range of 60 °C, and the GHSV values were changed from 9,000 to 18,000 h^{-1}. The concentration of ammonia in the outlet was quantitatively analyzed using a Shimadzu gas chromatograph (GC-2014) equipped with a TCD detector and a Thermon-3000 + KOH (2 + 2)% Sunpak-N 60/100 mesh column (2.1 m in length and 3.2 mm in internal diameter, Shinwa Chemical Industries Ltd., Japan). The ammonia synthesis rate (mmol g_{cat}^{-1} h^{-1}) was calculated by dividing the molar fraction of formed ammonia per gram of catalyst per unit time.

3. Results and discussion

3.1 Screening of the prepared catalysts

Fig. 1 shows the influence of the promotor on the catalytic performance of the prepared Ba-Ru and Cs-Ru catalysts with various Ba/Ru and Cs/Ru ratios during the ammonia synthesis, which was conducted in a fixed-bed reactor under a typical reaction condition. The H_2 pressure, H_2/N_2 ratio, GHSV value, and volume of the catalyst bed were maintained at 0.99 MPa, 3, 9,000 h^{-1}, and 0.8 mL, respectively. The reaction temperature was varied within the range of 280–550 °C. The ammonia synthesis rates were observed at the maxima of the curves shown in Fig. 1. The maxima ammonia synthesis rates and corresponding reaction temperatures are listed in Table 1. For the Ba-Ru catalysts, the increase in ammonia synthesis rate occurred in order of 0.5Ba-10Ru/AC < 0.1Ba-10Ru/MPC < 0.5Ba-10Ru/MPC. The 0.5Ba-10Ru/MPC catalyst provided the highest

Table 1 Catalytic performance over Ba-Ru and Cs-Ru catalysts at 0.99 MPa, H_2/N_2 = 3, GHSV = 9,000 h^{-1}.

Catalysts	Ammonia synthesis rate (mmol g_{cat}^{-1} h^{-1})	Ammonia synthesis rate (mmol g_{Ru}^{-1} h^{-1})	Ammonia yield (vol.%)	Temp. (°C)
0.5Ba-10Ru/MPC	79.1	977	2.4	410
0.1Ba-10Ru/MPC	59.5	668	1.8	430
0.5Ba-10Ru/AC	17.0	210	2.3	420
2.5Cs-10Ru/MPC	68.0	1015	3.4	400
0.5Cs-10Ru/MPC	43.2	508	1.4	460
0.1Cs-10Ru/MPC	24.8	275	0.7	520
2.5Cs-10Ru/AC	9.7	100	1.9	430

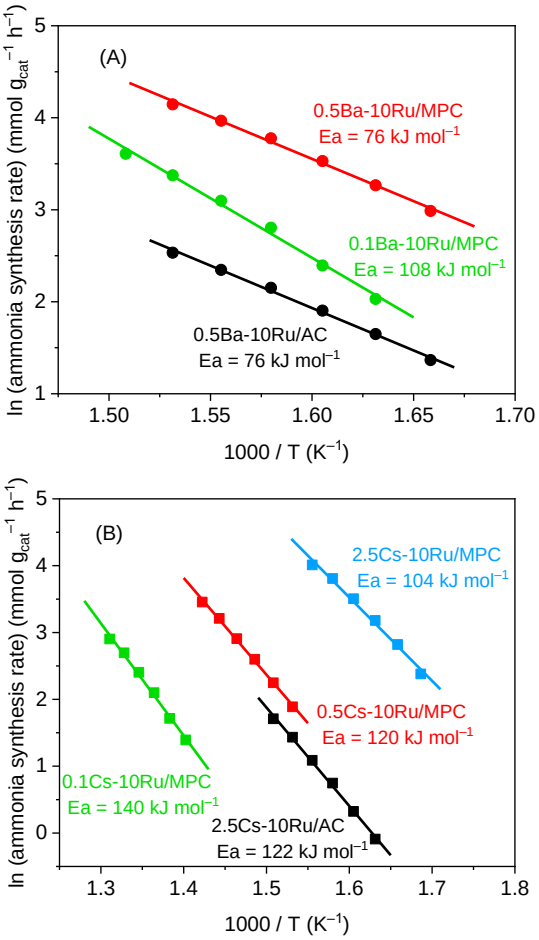

Fig. 2 Arrhenius plots for ammonia synthesis over (A) Ba-Ru and (B) Cs-Ru catalysts under mild conditions using a H_2 pressure of 0.99 MPa and a GHSV value of 9,000 h^{-1} using a mixed gas of H_2 and N_2 with a H_2/N_2 ratio of 3.

ammonia synthesis rate of 79.1 mmol g_{cat}^{-1} h^{-1} at 410 °C, corresponding to a NH_3 concentration of 2.4 vol.%. In contrast, the 0.1Ba-10Ru/MPC catalyst with a low Ba loading and the 0.5Ba-10Ru/AC catalyst with a densely microporous structure provided low ammonia synthesis rates at a relatively high temperature. Note that the density of the 0.5Ba-10Ru/AC catalyst is approximately 4-times higher than that of the 0.5Ba-10Ru/MPC catalyst. As a result, the 0.5Ba-10Ru/MPC catalyst provides a higher ammonia synthesis rate than that of the analogous catalyst of 0.5Ba-10Ru/AC at a similar ammonia yield. For the Cs-Ru catalysts, the increase in ammonia synthesis rate occurred in order of 2.5Cs-10Ru/AC < 0.1Cs-10Ru/MPC < 0.5Cs-10Ru/MPC < 2.5Cs-10Ru/MPC. Similarly, the 2.5Cs-10Ru/MPC catalyst provided the highest ammonia synthesis rate of 68.0 mmol g_{cat}^{-1} h^{-1} at 400 °C, corresponding to a NH_3 concentration of 3.4 vol.%. A decrease in the ammonia synthesis rate, through which the reaction temperature shifted to a higher temperature region, was observed for the 0.5Cs-10Ru/MPC and 0.1Cs-10Ru/MPC catalysts with low Cs loadings and the 2.5Cs-10Ru/AC catalyst with a microporous structure.

The Arrhenius plots for the temperature dependence of a mild ammonia synthesis over the prepared Ba-Ru and Cs-Ru catalysts are

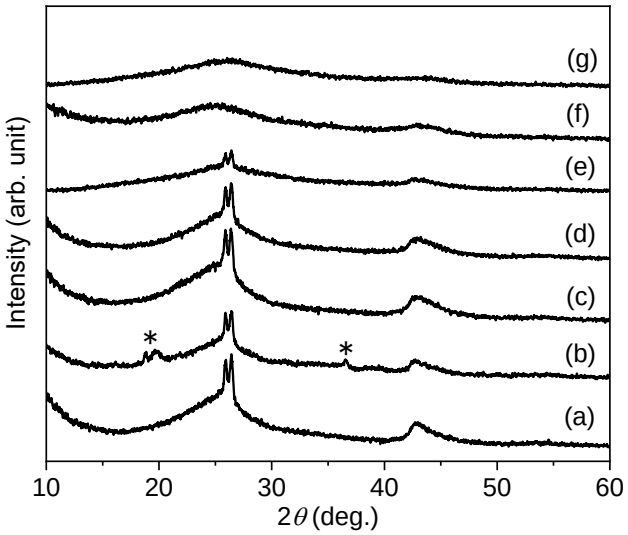

Fig. 3 Wide-angle XRD patterns of (a) 0.1Ba-10Ru/MPC, (b) 0.5Ba-10Ru/MPC, (c) 0.1Cs-10Ru/MPC, (d) 0.5Cs-10Ru/MPC, (e) 2.5Cs-10Ru/MPC, (f) 0.5Ba-10Ru/AC, and (g) 2.5Cs-10Ru/AC. The "asterisk" peaks arise from the $Ba(NO_3)_2$.

shown in Fig. 2, the data of which are calculated using the results of Fig. 1, and compared to the analogous catalysts without promoters (Fig. S2). The activation energy for a mild ammonia synthesis over 0.1Ba-10Ru/MPC and 0.5Ba-Ru/MPC varied within the range of 76–108 kJ mol^{-1}, and decreased with an increase in the Ba loading. Without Ba species, the 10Ru/MPC and 10Ru/AC catalysts showed a high activation energy of 153 and 168 kJ mol^{-1}, respectively, resulting in low activity in mild ammonia synthesis. Note that the activation energy of 0.5Ba-10Ru/MPC with a mesoporous structure is similar to that of an analogous catalyst of 0.5Ba-10Ru/AC with a microporous structure, whereas the ammonia synthesis rate over the 0.1–0.5Ba-10Ru/MPC catalyst is apparently higher. This result implies that the addition of Ba in the Ru-based catalysts can facilitate the ammonia synthesis through the reduction of the activation energy, which is probably related to the dissociation of N≡N bonding as the most difficult step during ammonia synthesis.[26] In addition, a higher ammonia synthesis rate over the 0.5Ba-10Ru/MPC catalyst should have to do with well-dispersed active sites with the aid of Ba promotion on the mesoporous structure, facilitating a molecular diffusion, in comparison to that of the 0.5Ba-10Ru/AC catalyst with a densely microporous structure, which hinders the molecular diffusion. Similarly, a decrease in the activation energy for the ammonia synthesis over the 0.1–2.5Cs-10Ru/MPC catalysts when increasing the Cs loading was observed, and the values (104–140 kJ mol^{-1}) were shown to be higher than those of the prepared Ba-Ru catalysts as aforementioned. For example, the activation energy for ammonia synthesis over 0.5Ba-10Ru/MPC is lower than that of 2.5Cs-10Ru/MPC, although their ammonia synthesis rates and yields are close to each other. It should also be noted that the 2.5Cs-10Ru/AC catalyst provides a higher activation energy of ammonia synthesis than that of the 2.5Cs-10Ru/MPC catalyst, which differs from the results of the prepared Ba-Ru catalysts. These observations indicate

Table 2 Structural properties of the prepared Ba-Ru and Cs-Ru catalysts and the reference materials.

Samples	Ru content (wt.%)	S_{BET} (m^2 g^{-1})	V_{Total} (cm^3 g^{-1})	V_{Micro} (cm^3 g^{-1})[a]	V_{Meso} (cm^3 g^{-1})[b]	Pore size (nm)	Ru size (nm)		TOF (h^{-1})
							HRTEM[c]	CO Chem.[d]	
0.5Ba-10Ru/MPC	8.1	660	1.68	0.26	1.42	5.4	1.9±0.5	3.2 (28.9%)	342 (410 °C)
0.1Ba-10Ru/MPC	8.9	810	1.91	0.34	1.57	5.4	1.9±0.6	2.1 (44.4%)	152 (430 °C)
0.5Ba-10Ru/AC	8.1	940	0.44	0.35	0.09	0.8	1.4±0.3	7.8 (11.8%)	180 (420 °C)
2.5Cs-10Ru/MPC	6.7	430	1.33	0.17	1.16	5.4	2.1±0.4	2.0 (45.8%)	224 (400 °C)
0.5Cs-10Ru/MPC	8.5	750	1.84	0.27	1.57	5.4	1.9±0.5	2.0 (45.0%)	114 (460 °C)
0.1Cs-10Ru/MPC	9.0	840	1.91	0.35	1.56	5.4	1.9±0.5	2.1 (44.2%)	63 (520 °C)
2.5Cs-10Ru/AC	6.7	580	0.30	0.24	0.06	0.8	1.6±0.4	6.2 (15.0%)	67 (430 °C)

[a] Microporous pore volume (V_{Micro}) was calculated using the Dubinin–Astakhov (DA) plot and the α_s-plot method.

[b] Mesoporous pore volume (V_{Meso}) was calculated as $V_{Total} - V_{Micro}$.

[c] Determined from the HRTEM images.

[d] Determined from CO chemisorption. The data in the parentheses are the Ru dispersions calculated through CO chemisorption.

that the promotors of Ba and Cs play different roles in mild ammonia synthesis over the prepared Ba-Ru and Cs-Ru catalysts, in addition to their structural properties. The influences of the promoters on the activity and durability of the 2.5Cs-10Ru/MPC and 0.5Ba-10Ru/MPC catalysts were studied at the molecular scale hereafter, in comparison to the analogous catalysts with a microporous structure.

3.2 Characterizations

Conventional techniques and X-ray absorption spectroscopy were utilized to survey the influences of the structural property and chemical environment on the catalytic performance of the prepared Ba-Ru and Cs-Ru catalysts during mild ammonia synthesis, particularly for long-term operations under the intermittently varied conditions applied in this study. The PXRD patterns in Fig. 3 show that all samples contain two groups of X-ray diffraction signals at 2θ = 25–26° and 44–45°, corresponding to a layer structure of graphite derived from the supporting material of MPC.[27] No Ru species are visible in the PXRD patterns, suggesting that small Ru particles with an amorphous nature are only impregnated on the MPC. A similar phenomenon is observed for the Cs species. However, Ba in the form of $Ba(NO_3)_2$, the Ba precursor, is observed at 2θ = 18.9° and 36.6°, suggesting that the chemical environment of Ba on the MPC is not affected by the impregnation and its particle size can be reduced to the nanometer scale. The HRTEM images in Fig. 4 show that all samples contain well-dispersed Ru particles with average sizes of ~2 nm (also see Table 2 and ESI, Fig. S3). The 0.1–0.5Ba-10Ru/MPC and 0.1–2.5Cs-10Ru/MPC catalysts contain an open mesoporous carbon framework, whereas the 0.5Ba-10Ru/AC and2.5Cs-10Ru/AC catalysts only have a dense carbon framework. Note that the Ru sizes are much smaller than the pore sizes of 0.1–0.5Ba-10Ru/MPC and 0.1–2.5Cs-10Ru/MPC catalysts, as analyzed through the N_2 adsorption–

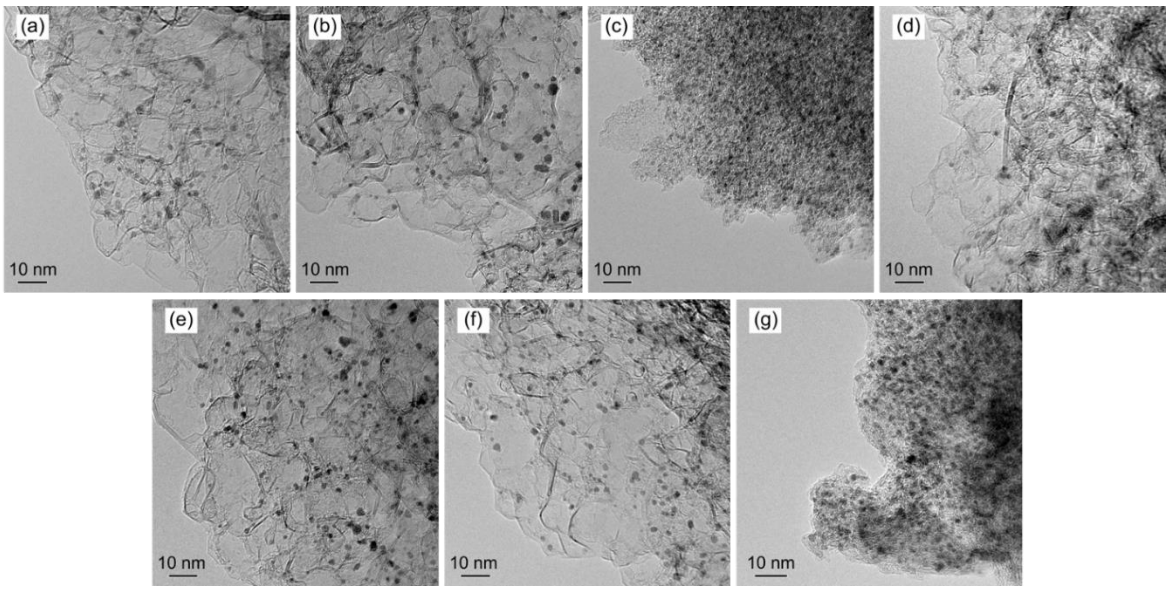

Fig. 4 HRTEM images of (a) 0.5Ba-10Ru/MPC, (b) 0.1Ba-10Ru/MPC, (c) 0.5Ba-10Ru/AC, (d) 2.5Cs-10Ru/MPC, (e) 0.5Cs-10Ru/MPC, (f) 0.1Cs-10Ru/MPC, and (g) 2.5Cs-10Ru/AC.

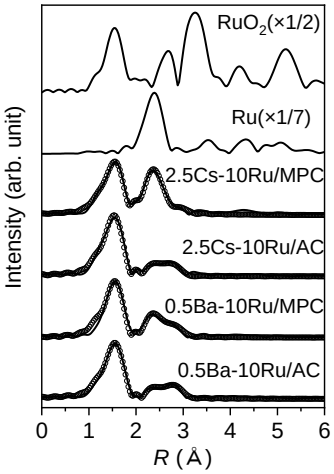

Fig. 5 Fourier transforms of Ru *K*-edge EXAFS spectra for prepared Ba-Ru and Cs-Ru catalysts and standard metallic Ru and RuO_2. The solid lines are the experiment data, whereas the empty circles are the fitted results within an *R*-range of 1.0–3.0 Å.

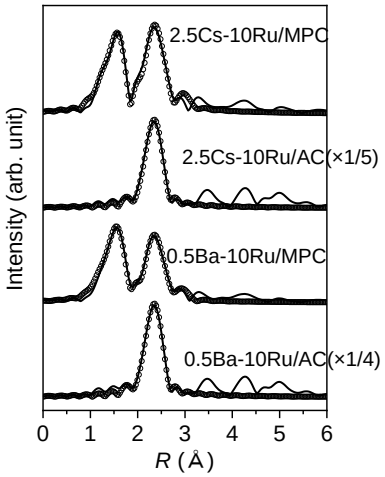

Fig. 6 Fourier transforms of Ru *K*-edge EXAFS spectra for used Ba-Ru and Cs-Ru catalysts. The solid lines indicate the experiment data, whereas the empty circles are the fitted results within the *R*-range of 1.0–3.0 Å.

desorption isotherm and pore size calculation (Table 2 and ESI, Fig. S4). It can be stated that the Ru particles should be impregnated inside the mesopores of these catalysts. In contrast, the Ru sizes within the range of 1.4–1.6 nm are larger than those of the micropores (~0.8 nm) of 0.5Ba-10Ru/AC and 2.5Cs-10Ru/AC. The Ru particles are close to each other, as shown in Fig. 4(c) and (g). This implies that the Ru particles are presumably impregnated on the pore mouths of 0.5Ba-10Ru/AC and 2.5Cs-10Ru/AC in the outside structure rather than in the pores in the inner structure.

The CO chemisorption technique was utilized to study the Ru sizes of the prepared Ba-Ru and Cs-Ru catalysts after a reduction treatment at 450 °C for 2 h. Note that the reduction condition for the CO chemisorption experiment was akin to that for a mild ammonia synthesis, as mentioned in the section 2.3. Table 2 shows that the Ru sizes of the 0.1–2.5Cs-10Ru/MPC catalysts calculated using the CO chemisorption were approximately 2 nm, which are close to the results from the HRTEM images. This indicates that the reduction treatment has no significant influence on the Ru sizes of the 0.1–

Table 3 Structural parameters of the environment of Ru atoms in prepared Ba-Ru and Cs-Ru catalysts and reference materials obtained through the fitting of Ru *K*-edge EXAFS spectra under ambient conditions.

Catalysts	Shell	N^a	R (Å)^b	ΔE (eV)^c	σ^2 (Å^2)^d
0.5Ba-10Ru/MPC	Ru-O (RuO_2)	3.2±0.6	2.02±0.01	1.7±2.6	0.0055±0.0018
	Ru-Ru (RuO_2)	1.1±0.2	3.15±0.01	1.5±1.2	0.0090±0.0023
	Ru-Ru (metal)	2.7±0.8	2.71±0.02	–3.3±2.8	0.0118±0.0027
0.5Ba-10Ru/AC	Ru-O (RuO_2)	3.3±0.5	2.02±0.01	4.8±1.4	0.0067±0.0010
	Ru-Ru (RuO_2)	1.2±0.1	3.15±0.01	4.7±0.7	0.0100±0.0016
	Ru-Ru (metal)	2.0±0.6	2.73±0.02	2.9±2.6	0.0142±0.0032
2.5Cs-10Ru/MPC	Ru-O (RuO_2)	3.3±0.5	2.01±0.01	4.5±1.8	0.0072±0.0016
	Ru-Ru (RuO_2)	1.1±0.2	3.14±0.02	4.2±1.0	0.0100±0.0020
	Ru-Ru (metal)	3.0±0.5	2.69±0.01	–2.3±1.5	0.0083±0.0011
2.5Cs-10Ru/AC	Ru-O (RuO_2)	3.6±0.5	2.01±0.01	4.0±2.1	0.0063±0.0015
	Ru-Ru (RuO_2)	1.2±0.2	3.14±0.03	4.0±1.2	0.0126±0.0030
	Ru-Ru (metal)	2.0±0.8	2.74±0.01	3.2±2.2	0.0138±0.0055
RuO_2	Ru-O	6	1.97±0.04	0.9±2.4	0.0035±0.0008
	Ru-Ru	2	3.11±0.01	–0.6±1.8	0.0028±0.0007
Ru(metal)	Ru-Ru	12	2.68±0.01	3.3±1.6	0.0044±0.0003

[a] Coordination number, [b] Interatomic distance, [c] Inner potential correction, [d] Debye-Waller factor

Table 4 Structural parameters of the environment of Ru atoms in used Ba-Ru and Cs-Ru catalysts and reference materials obtained through the fitting of Ru *K*-edge EXAFS spectra under ambient conditions.

Catalysts	Shell	N^a	R (Å)^b	ΔE (eV)^c	σ^2 (Å^2)^d
0.5Ba-10Ru/MPC	Ru-O (RuO_2)	3.1±0.5	2.01±0.01	3.5±2.1	0.0073±0.0018
	Ru-Ru (RuO_2)	1.0±0.1	3.16±0.01	3.2±1.2	0.0103±0.0021
	Ru-Ru (metal)	2.7±0.4	2.69±0.01	–3.7±1.6	0.0079±0.0011
0.5Ba-10Ru/AC	Ru-Ru (metal)	7.7±0.4	2.68±0.01	2.9±2.6	0.0050±0.0003
2.5Cs-10Ru/MPC	Ru-O (RuO_2)	3.3±0.6	2.01±0.01	4.4±2.1	0.0072±0.0019
	Ru-Ru (RuO_2)	1.1±0.2	3.15±0.02	4.1±0.9	0.0076±0.0017
	Ru-Ru (metal)	2.2±0.4	2.70±0.01	–2.3±1.5	0.0051±0.0011
2.5Cs-10Ru/AC	Ru-Ru (metal)	8.3±0.4	2.68±0.01	–5.5±0.8	0.0046±0.0003

[a] Coordination number, [b] Interatomic distance, [c] Inner potential correction, [d] Debye-Waller factor

2.5Cs-10Ru/MPC catalysts. The Ru sizes of the 0.1–0.5Ba-10Ru/MPC catalysts were approximately 2–3 nm, which were slightly larger than the results of the HRTEM images. The Ru sizes were presumably overestimated through the CO chemisorption owing to the hinderance of the Ba species stuck on the Ru surface.[21] For the 0.5Ba-10Ru/AC and 2.5Cs-10Ru/AC catalysts, the Ru sizes are significantly increased to 6–8 nm, as determined using the CO chemisorption technique. This observation is similar to those found in our recent studies.[19–21] The Ru particles are presumably impregnated on the pore mouths of the 0.5Ba-10Ru/AC and 2.5Cs-10Ru/AC catalysts, and thus they aggregate easily through a reduction treatment, which was used in the CO chemisorption and ammonia synthesis.

3.3 X-ray absorption spectroscopy

The chemical environments of freshly-prepared and used Ba-Ru and Cs-Ru catalysts were further studied using Ru *K*-edge X-ray absorption spectroscopy, in comparison to the reference materials of Ru metal and RuO_2, containing a rutile structure with a purity of >98%. RuO_2 was purchased from Wako Co. Ltd., Japan. The corresponding Fourier transforms of the k^3-weighted spectra in the *R* space are shown in Figs. 5 and 6. The *K*-edge spectrum of Ru metal with a hexagonal close-packed structure show a characteristic peak at 22.126 keV, which is assigned to the electron transition from an initial state of a 1s energy level to the excited states of a predominately 5p characteristic (Fig. S5). The Fourier transform of the Ru *K*-edge spectrum of the Ru metal shows an intense peak at 2.4 Å (uncorrected, Fig. 5). The fitting of the spectrum shows that Ru metal contains a coordination of 12 and a Ru-Ru distance of 2.68±0.01 Å. Regarding the rutile RuO_2, several peaks at 1.6, 2.8, 3.4, and 4.2 Å (uncorrected, Fig. 5) are observed in the Fourier transform of the Ru *K*-edge spectrum. The fitting of the spectrum shows that RuO_2 contains a Ru-O shell with a coordination of 6 and a Ru-Ru shell with a coordination number of 2. These results are consistent with the literature reports and are used as reference data hereafter.[28]

All freshly prepared Ba-Ru and Cs-Ru catalysts show two groups of signals at approximately 1.6 and 2.4–2.8 Å (uncorrected) in the Fourier transforms of the Ru *K*-edge EXAFS spectra. One group which shows two signals at 1.6 and 2.8 Å (uncorrected) is associated with the Ru-O and Ru-Ru shells of RuO_2 particles, and the corresponding coordination numbers are much smaller than those of RuO_2 fine powder, as previously mentioned. It is clear that the freshly prepared Ba-Ru and Cs-Ru catalysts contain nano-sized RuO_2 particles, which are consistent with the PXRD and HRTEM studies. By contrast, a signal at 2.4 Å (uncorrected), which is associated with the Ru-Ru shell of metallic Ru, can be observed, particularly for the freshly prepared Cs-Ru catalysts. The Ba-Ru/MPC and Cs-Ru/MPC catalysts were prepared through a stepwise impregnation of Ba, Cs and Ru precursors on the MPC. In the first step used to obtain the Ru/MPC catalysts, the Ru precursors, which were impregnated on the MPC, were presumably decomposed into a metallic Ru species by calcining at 400 °C in N_2, and re-oxidized into nano-sized RuO_2 particles when exposed to air. In the second step conducted to obtain the Ba-Ru/MPC and Cs-Ru/MPC catalysts, the Ba and Cs precursors were impregnated on the Ru/MPC catalysts, and dried until all solvents were evaporated. As shown in Fig. 5, the Ru-Ru shell of the metallic Ru species suggests that a small portion of the species presumably exists in the core of the RuO_2 particles, corresponding to RuO_x

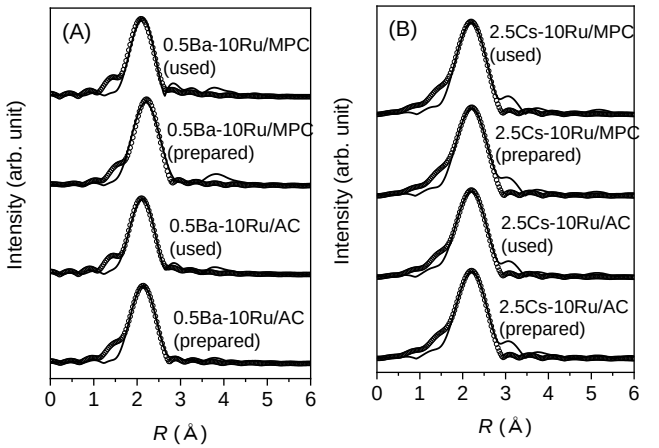

Fig. 7 Fourier transforms of Ba and Cs *K*-edge EXAFS spectra for prepared and used (A) Ba-Ru and (B) Cs-Ru catalysts. The solid lines indicate the experiment data, whereas the empty circles are the fitted results conducted within the *R*-range of 1.0–3.0 Å.

Table 5 Structural parameters of the environment of Ba and Cs atoms in prepared and used Ba-Ru and Cs-Ru catalysts obtained through the fitting of Ba or Cs *K*-edges EXAFS spectra under ambient conditions.

Catalysts	Shell	N^a	R (Å)^b	ΔE (eV)^c	σ^2 (Å^2)^d
$Ba(NO_3)_2$ standard	Ba-O	10	2.88±0.02	2.8±1.6	0.0075±0.0027
BaO standard[30]	Ba-O	6	2.78±0.03	-1.3±2.5	0.0135±0.0037
0.5Ba-10Ru/MPC (prepared)	Ba-O	4.5±0.8	2.85±0.02	2.8±2.0	0.0130±0.0032
0.5Ba-10Ru/MPC (used)	Ba-O	3.1±0.7	2.75±0.02	–0.8±2.4	0.0099±0.0037
	Ba-O^e	3.7±0.4^e	2.75±0.03^e	-0.7±2.7^e	0.013^e
0.5Ba-10Ru/AC (prepared)	Ba-O	4.1±0.9	2.79±0.02	1.3±2.1	0.0142±0.0041
0.5Ba-10Ru/AC (used)	Ba-O	3.0±0.4	2.76±0.01	–1.1±1.3	0.0095±0.0020
	Ba-O^e	4.0±0.4^e	2.76±0.03^e	-1.4±2.6^e	0.014^e
2.5Cs-10Ru/MPC (prepared)	Cs-O	3.7±1.4	2.98±0.06	–4.8±4.8	0.0245±0.0121
2.5Cs-10Ru/MPC (used)	Cs-O	3.6±1.4	2.97±0.06	–5.3±4.7	0.0228±0.0112
2.5Cs-10Ru/AC (prepared)	Cs-O	3.3±1.3	2.97±0.06	–4.7±4.6	0.0225±0.0112
2.5Cs-10Ru/AC (used)	Cs-O	3.2±1.2	2.97±0.06	–4.8±4.5	0.0221±0.0108

[a] Coordination number, [b] Interatomic distance, [c] Inner potential correction, [d] Debye-Waller factor, [e] Debye-Waller factor was set at 0.013–0.014 for comparison.

particles with a RuO_2-shell and a Ru-core in all Ba-Ru and Cs-Ru catalysts, particularly for the 2.5Cs-10Ru/MPC catalyst. The ratios of metallic and oxide components in the prepared Ba-Ru and Cs-Ru catalysts were estimated by analysis of XANES spectra using a linear combination fitting method (Fig. S5 and Table S1). The results show that the component of RuO_2 in the prepared Ba-Ru and Cs-Ru catalysts are higher than that of metallic species, which are in good agreement with the EXAFS analysis.

The used Ba-Ru and Cs-Ru catalysts were collected after the ammonia synthesis, during which they were exposed to air under ambient conditions, and then studied using Ru *K*-edge EXAFS spectroscopy. The Fourier transforms of the Ru *K*-edge EXAFS spectra and the corresponded fitting data are shown in Fig. 6 and Table 4, respectively. For the used 0.5Ba-10Ru/AC and 2.5Cs-10Ru/AC catalysts, an intense signal corresponding to the Ru-Ru shell of metallic Ru particles with coordination numbers of 7–8 was only observed. This implies that the Ru species of the used 0.5Ba-10Ru/AC and 2.5Cs-10Ru/AC catalysts aggregated into large Ru particles, which are unreactive to oxygen molecules when exposed to air under ambient conditions. In contrast, the Fourier transforms of the Ru *K*-edge EXAFS spectra of the used 0.5Ba-10Ru/MPC and 2.5Cs-10Ru/MPC catalysts were similar to those of freshly prepared samples, although the coordination numbers slightly increased. This result indicates that the nano-sized Ru species on the 0.5Ba-10Ru/MPC and 2.5Cs-10Ru/MPC catalysts are stable under redox conditions (before and after the ammonia synthesis), which are also consistent with the HRTEM study.

The chemical environments of the Ba and Cs species in the freshly prepared and used 0.5Ba-10Ru/MPC and 2.5Cs-10Ru/MPC catalysts were also studied based on the Ba and Cs *K*-edge EXAFS spectra, in comparison to those of the analogous catalysts of 0.5Ba-10Ru/AC and 2.5Cs-10Ru/AC (Fig. 7 and Table 5), and standards of $Ba(NO_3)_2$ and BaO[30]. For the freshly prepared Ba-Ru and Cs-Ru catalysts, an intense signal corresponding to a Ba-O or Cs-O shell is observed in the Fourier transforms of the Ba or Cs *K*-edge spectra, respectively.[29] The coordination number of the Ba-O shell in the 0.5Ba-10Ru/MPC catalyst is slightly higher than that of the Cs-O shell in the 2.5Cs-10Ru/MPC catalyst. Similar results were observed for the freshly prepared 0.5Ba-10Ru/AC and 2.5Cs-10Ru/AC catalysts. It is another indication that relatively large Ba species in the form of $Ba(NO_3)_2$ are existence in the freshly prepared 0.5Ba-10Ru/MPC and 0.5Ba-10Ru/AC catalysts, as supported through a PXRD analysis. For the used Ba-Ru and Cs-Ru catalysts, the signal of the Ba-O or Cs-O shell is slightly decreased, corresponding to relatively small coordination numbers, particularly for the used Ba-Ru catalysts. This implies that small BaO_x and CsOH species are formed through the decomposition of Cs and Ba precursors impregnated on the Ba-Ru and Cs-Ru catalysts during the ammonia synthesis and stably exist even after exposure to air.

The chemical states of Cs species of freshly prepared and used Cs-Ru catalysts had been thoroughly studies by TPR-MS techniques and several conventional characterizations.[20] It is generally agreed that Cs_2CO_3 impregnated on the activated carbon or mesoporous carbon-supported Ru catalysts was converted to CsOH species in the reduced atmosphere, and CsOH plays as an electronic promotor for Ru-catalyzed ammonia synthesis. However, the chemical states and roles of Ba species in the supported Ba-Ru catalysts for ammonia synthesis are still controversial. In this study, the chemical state of Ba species in the freshly prepared Ba-Ru catalysts, especially 0.5Ba-10Ru/MPC, is different from that of used samples. The XRD patterns show that the Ba species in the form of $Ba(NO_3)_2$ are impregnated on the freshly prepared Ba-Ru catalysts, especially for 0.5Ba-10Ru/MPC, and it probably converts to BaO with a small portion of $BaCO_3$ for the used samples after exposed to air. Noted that $BaCO_3$ is formed by the

reaction of BaO with CO_2 molecules in the atmosphere.[21] This speculation is supported by the previous study of Zeng *et al*.[31] They utilized the TGA-MS technique to study the chemical states of $Ba(NO_3)_2$ impregnated on the activated carbon-supported Ru catalysts, and concluded that $Ba(NO_3)_2$ was converted to BaO during the ammonia synthesis and to BaOH after the reaction and exposed to moist air. In Table 5, our EXAFS data further show that the coordination numbers of Ba-O shell are around 4.1–4.5 with interatomic distances of 2.79–2.85 Å for freshly prepared 0.5Ba-10Ru/MPC and 0.5Ba-10Ru/AC catalysts, which are similar to the structural parameters of $Ba(NO_3)_2$ standard. For the used 0.5Ba-10Ru/MPC and 0.5Ba-10Ru/AC catalysts, the coordination numbers of Ba-O shell are decreased to 3.0–3.1 with interatomic distances of 2.75–2.76 if the Debye-Waller factor are not fixed. These structural parameters are similar to those of BaO standard. We also tried to set the ss values at 0.013–0.014, and found that the coordination numbers of Ba-O shell are slightly increased to 3.7–4.0. However, the other parameters, such as interatomic distance and inner potential correction, are still closed to those of BaO standard. Slightly high coordination number of Ba-O shell in the used 0.5Ba-10Ru/AC catalyst should be associated with relatively large BaO particles with a small portion of $BaCO_3$. This speculation is supported by the XRD pattern (Fig. S6 in ESI) and EXAFS analysis. In other words, high coordination numbers of Ba in the prepared 0.5Ba-10Ru/MPC and 0.5Ba-10Ru/AC catalysts are presumably due to the existence of $Ba(NO_3)_2$. Relatively low coordination numbers of Ba in the used samples are associated with the existence of BaO particles with a small portion of $BaCO_3$. In combination of the findings of X-ray absorption spectroscopy with other characterizations, it can be stated that small BaO_x species, formed by the reduction of $Ba(NO_3)_2$, are likely adhered on the nano-sized Ru^0 particles, which presumably formed more catalytically active sites on the surfaces, such as B_5 sites, facilitating the dissociation of nitrogen molecules for mild ammonia synthesis. By contrast, small CsOH species, formed by the reduction of Cs_2CO_3, are likely covered on the mesoporous carbon and Ru interfaces, forming Ru^0 active sites with enhanced electronic property for mild ammonia synthesis.

3.4 Long-term ammonia synthesis under intermittently variation conditions

The long-term ammonia synthesis of the 0.5Ba-10Ru/MPC and 2.5Cs-10Ru/MPC was studied using a fixed-bed reactor equipped with a quartz inlet under intermittently variation conditions, in comparison to the 0.5Ba-10Ru/AC and 2.5Cs-10Ru/AC. The results are shown in Figs. 8 and 9. The volume of the catalyst bed was kept at 0.8 mL. The reaction temperatures for the 0.5Ba-10Ru/MPC, 0.5Ba-10Ru/AC, 2.5Cs-10Ru/MPC, and 2.5Cs-10Ru/AC was set at 410, 420, 400 and 430 °C, respectively, corresponding to the maxima ammonia synthesis rates, as observed in Fig. 1. The reaction temperature was varied within the range of 60 °C based on the reaction temperatures, as previously mentioned. The GHSV value was varied between 9,000 and 18,000 h^{-1}. The reaction pressure was kept at 0.99 MPa. For example, the reaction temperature and GHSV value of the 0.5Ba-10Ru/MPC catalyst during a mild ammonia synthesis were varied within 350–410 °C and 9,000–18,000 h^{-1}, respectively. Fig. 8 shows that the ammonia synthesis rate over the 0.5Ba-10Ru/MPC catalyst can be quickly tuned at ranges of 30.5–77.0 mmol g_{cat}^{-1} h^{-1} (0.9–2.3

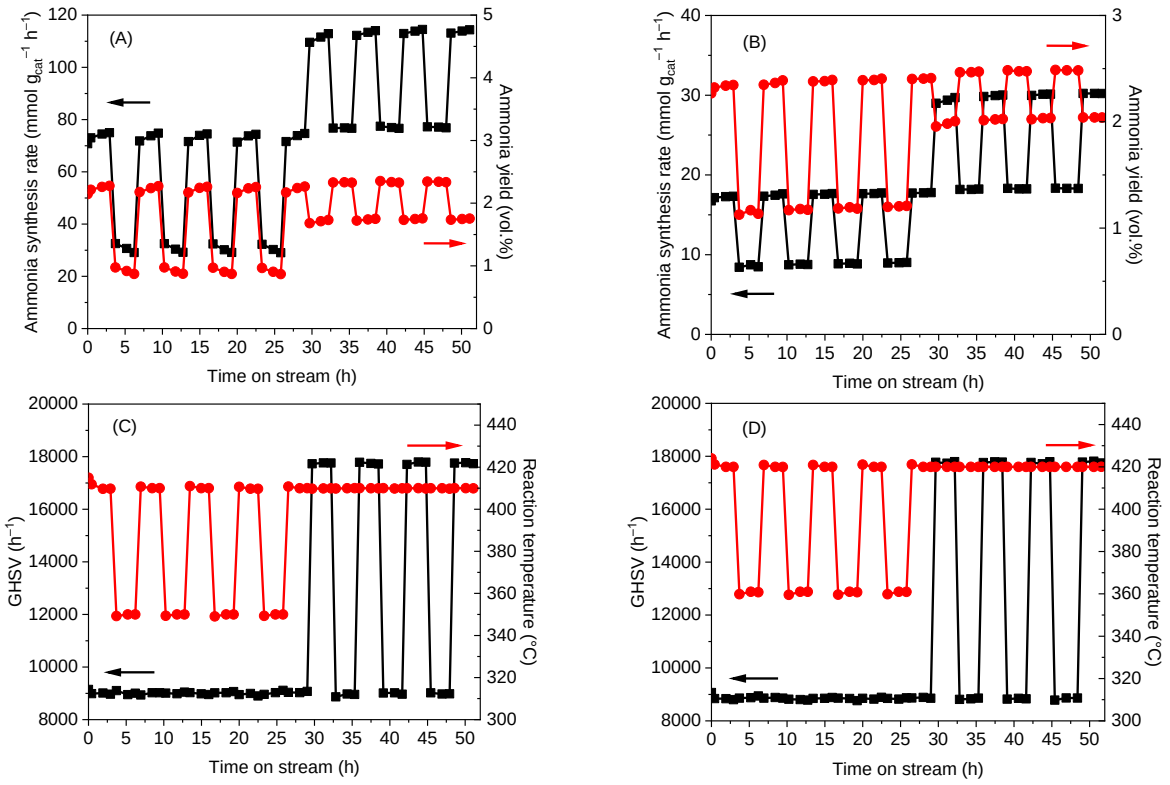

Fig. 8 Long-term ammonia synthesis over (A, C) 0.5Ba-10Ru/MPC and (B, D) 0.5Ba-10Ru/AC under intermittently varying conditions.

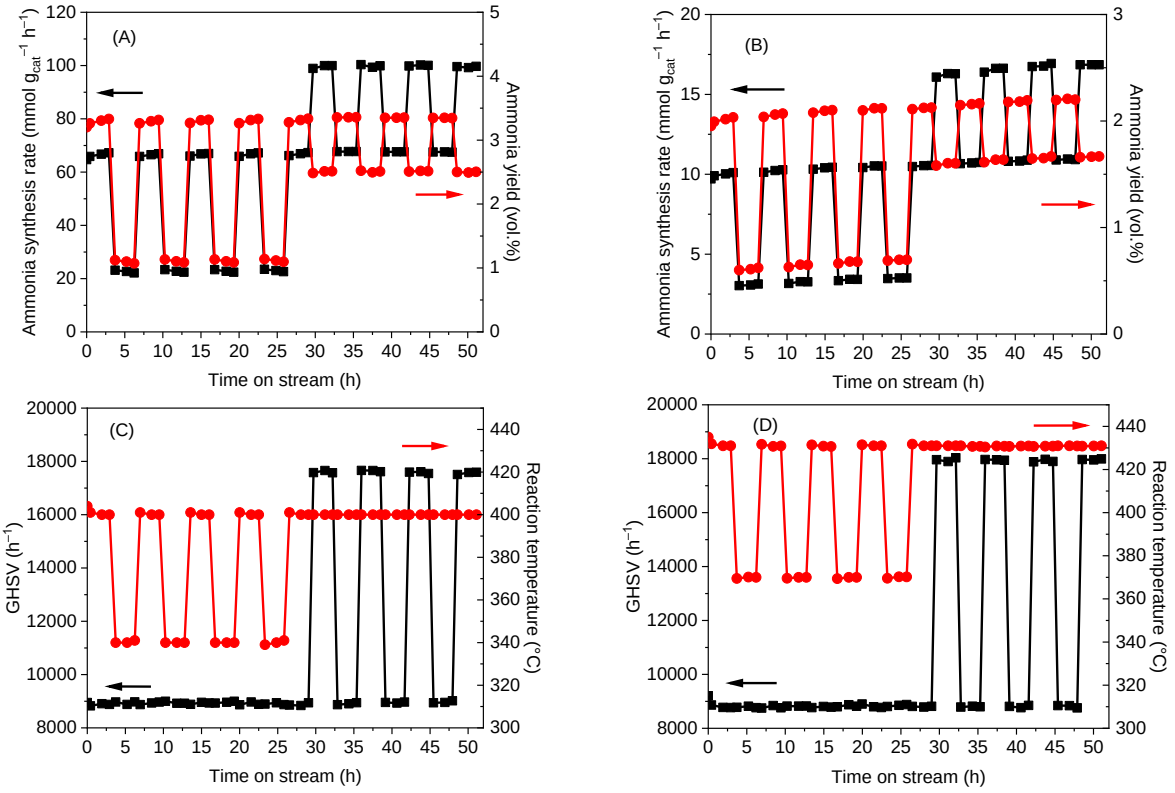

Fig. 9 Long-term ammonia synthesis over (A, C) 2.5Cs-10Ru/MPC and (B, D) 2.5Cs-10Ru/AC under intermittently varying conditions.

vol.%) and 77.0–114 mmol g_{cat}^{-1} h^{-1} (1.7–2.3 vol.%) by varying the reaction temperature and GHSV values within a short reaction period (3 h) for at least eight cycles. The ammonia yield was ~2.3 vol.% with a variation of 3.8% under conditions of 410 °C and 9,000 h^{-1} for more than 50 h and eight cycles. Similar phenomenon can be observed for the 0.5Ba-10Ru/AC catalyst with a microporous structure, although the ammonia synthesis rate and yield are significantly decreased to 17.2 mmol g_{cat}^{-1} h^{-1} and 2.3 vol.%. It should be noted in particular that the ammonia synthesis yield over the 0.5Ba-10Ru/AC catalyst was 2.3–2.5 vol.% with a variation of 5.6% under conditions of 420 °C and 9,000 h^{-1} for more than 50 h and eight cycles. This implies that the ammonia synthesis over the 0.5Ba-10Ru/AC catalyst with a microporous structure is relatively unstable compared with that of the 0.5Ba-10Ru/MPC catalyst with a mesoporous structure after a time-on-stream of more than 50 h.

Similar results were observed for the 2.5Cs-10Ru/MPC catalyst. The ammonia synthesis rate and yield can be finely and stably tuned within the ranges of 22.5–67.5 mmol g_{cat}^{-1} h^{-1} (1.1–3.4 vol.%) and 67.5–100 mmol g_{cat}^{-1} h^{-1} (2.5–3.4 vol.%) by varying the reaction temperature and GHSV values within a short timeframe of approximately 3 h for at least eight cycles. The variation in the ammonia synthesis yield over the 2.5Cs-10Ru/MPC catalyst is reduced to 1.5% under the conditions of 400 °C and 9,000 h^{-1} for more than 50 h and eight cycles. However, the ammonia synthesis rate and yield over the 2.5Cs-10Ru/AC catalyst decreased to 10.0 mmol g_{cat}^{-1} h^{-1} (2.0 vol.%) and varied significantly (8.6%) as the reaction time was prolonged, indicating that the ammonia synthesis does not reach a steady state. In other words, the Ba-Ru/MPC, and in particular, the Cs-Ru/MPC catalysts are able to stably catalyze the ammonia synthesis under intermittently varying conditions, as compared with the Cs-Ru/AC and Ba-Ru/AC catalysts, presumably owing to a lower sintering and better molecular diffusion capability of catalytically active sites confined inside the mesoporous carbon frameworks.

Conclusions

The 0.5Ba-10Ru/MPC and 2.5Cs-10Ru/MPC catalysts were prepared through a stepwise impregnation of Ru (10 wt.%) and its promotors (Ba (Ba/Ru = 0.5) or Cs (Cs/Ru = 2.5)) on commercial mesoporous carbon (i.e., MPC), and applied to a mild ammonia synthesis, the results of which were compared to several reference catalysts with different Ba/Ru and Cs/Ru loadings and porous structures. According to the X-ray absorption spectroscopy and the fitting of the EXAFS region, the catalytically active sites of the 0.5Ba-10Ru/MPC catalyst were associated with BaO_x adhered to the nano-sized Ru surfaces, which presumably formed more B_5 sites, facilitating the dissociation of nitrogen molecules as a rate-determining step for an ammonia synthesis. In contrast, the 2.5Cs-10Ru/MPC catalyst contained CsOH homogeneously impregnated on the interfaces of the Ru and mesoporous carbon material, which improved the electronic property of the nano-sized Ru particles, and therefore facilitated an ammonia synthesis. The mesoporous carbon framework was able to stably confine these catalytically active sites in the nano-spaces during ammonia synthesis and even after ammonia synthesis upon exposure to air. As a result, a mild ammonia synthesis over the 0.5Ba-

10Ru/MPC and 2.5Cs-10Ru/MPC catalysts with catalytically active sites stably confined inside the mesoporous carbon frameworks could be well-adjusted under the intermittently varied conditions to simulate the variable hydrogen production derived from the electrolysis of water using renewable electricity, particularly for 2.5Cs-10Ru/MPC. The reference catalysts of 0.5Ba-10Ru/AC and 2.5Cs-10Ru/AC provided a low activity and yields under mild ammonia synthesis and were relatively unstable under the intermittently varying conditions, presumably owing to the sintering of these active sites on the outer surfaces of the microporous carbon frameworks.

Conflicts of interest

There are no conflicts to declare.

Acknowledgements

The authors acknowledge financial support from the Council for Science, Technology, and Innovation (CSTI), the Cross-ministerial Strategic Innovation Promotion Program (SIP), and the Energy Carriers program funded by JST. This work is partially supported by the Photon Factory Program Advisory Committee (Proposal no. 2017G613). Furthermore, the authors would like to express their gratitude to Mr. Akira Takatsuki of RIEF, AIST, for facilitating the HRTEM measurements, Dr. Koji Kuramoto of RIEF, AIST, for assistance with the PXRD measurements, and Dr. Takehisa Mochizuki of RIEF, AIST, for his help constructing the CO chemisorption instrument. Special thanks to Editage (https://www.editage.jp/) for the English language editing.

Notes and references

1 A. Grubler, C. Wilson, N. Bento, B. Boza-Kiss, V. Krey, D. L. McCollum, N. D. Rao, K. Riahi, J. Rogelj, S. De Stercke, J. Cullen, S. Frank, O. Fricko, F. Guo, M. Gidden, P. Havlík, D. Huppmann, G. Kiesewetter, P. Rafaj, W. Schoepp and H. Valin, *Nat. Energy*, 2018, **3**, 515–527.
2 Japan Metrological Agency, Carbon Dioxide (CO2), JMA Observation, http://www.data.jma.go.jp/ghg/kanshi/ghgp/co2_e.html.
3 United Nations Framework Convention on Climate Change (UNFCCC). Paris agreement, https://unfccc.int/sites/default/files/english_paris_agreement.pdf.
4 O. Kurata, N. Iki, T. Matsunuma, T. Inoue, T. Tsujimura, H. Furutani, H. Kobayashi and A. Hayakawa, *Proc. Combus. Inst.*, 2017, **36**, 3351–3359.
5 V. Smil, *Nature*, 1999, **400**, 415.
6 JGC Corporation, World's first successful ammonia synthesis using renewable energy-based hydrogen and power generation, https://www.jgc.com/en/news/assets/pdf/20181019e.pdf.
7 A. Ozaki, K. Aika and H. Hori, *Bull. Chem. Soc. Jap.*, 1971, **44**, 3216.
8 K. Aika, H. Hori and A. Ozaki, *J. Catal.*, 1972, **27**, 424–431.
9 M. Hattori, T. Mori, T. Arai, Y. Inoue, M. Sasase, T. Tada, M. Kitano, T. Yokoyama, M. Hara and H. Hosono, *ACS Catal.*, 2018, **8**, 10977–10984.
10 M. Kitano, Y. Inoue, M. Sasase, K. Kishida, Y. Kobayashi, K. Nishiyama, Y. Tada, S. Kawamura, T. Yokoyama, M. Hara and H. Hosono, *Angew. Chem. Int. Ed.*, 2018, **57**, 2648–2652.
11 M. Kitano, S. Kanbara, Y. Inoue, N. Kuganathan, P.V. Sushko, T. Yokoyama, M. Hara and H. Hosono, *Nat. Commun.*, 2015, **6**, 6731.
12 K. Sato, K. Imamura, Y. Kawano, S. Miyahara, T. Yamamoto, S. Matsumura and K. Nagaoka, *Chem. Sci.*, 2017, **8**, 674–679.
13 Y. Ogura, K. Tsujimaru, K. Sato, S. Miyahara, T. Toriyama, T. Yamamoto, S. Matsumura and K. Nagaoka, *ACS Sustainable Chem. Eng.*, 2018, **6**, 2230–2237.
14 W. Raróg-Pilecka, E. Miśkiewicz, D. Szmigiel and Z. Kowalczyk, *J. Catal.*, 2005, **231**, 11–19.
15 W. Raróg-Pilecka, E. Miśkiewicz, S. Jodzis, J. Petryk, D. Łomot, Z. Kaszkur, Z. Karpiński and Z. Kowalczyk, *J. Catal.*, 2006, **239**, 313–325.
16 I. Rossetti, F. Mangiarini and L. Forni, *Appl. Catal. A-Gen.*, 2007, **323**, 219–225.
17 I. Rossetti, N. Pernicone and L. Forni, *Catal. Today*, 2005, **102–103**, 219–224.
18 X. Wang, X. Peng, Y. Zhang, J. Ni, C. Au and L. Jiang, *Inorg. Chem. Front.*, 2019, **6**, 396–406.
19 M. Nishi, S.Y. Chen and H. Takagi, *ChemCatChem*, 2018, **10**, 3411–3414.
20 M. Nishi, S.Y. Chen and H. Takagi, *Catalysts*, 2019, **9**, 406.
21 M. Nishi, S.Y. Chen and H. Takagi, *Catalysts*, 2019, **9**, 480.
22 S.G. Chen and R.T. Yang, *Langmuir*, 1994, **10**, 4244–4299.
23 N. Setoyama, T. Suzuki and K. Kaneko, *Carbon*, 1998, **36**, 1459–1467.
24 B. Ravel and M. Newville, *J. Synchrotron Radiat.*, 2005, **12**, 537–541.
25 S.I. Zabinsky, J.J. Rehr, A. Ankudinov, R.C. Albers and M.J. Eller, *Phys. Rev. B*, 1995, **52**, 2995–3009.
26 T.W. Hansen, P.L. Hansen, S. Dahl and C.J.H. Jacobsen, *Catal. Lett.*, 2002, **84**, 7–12.
27 N. Kasahara, S. Shiraishi and A. Oya, *Carbon*, 2003, **41**, 1654–1656.
28 Z.R. Cormier, H.A. Andreas and P. Zhang, *J. Phys. Chem. C*, 2011, **115**, 19117–19128.
29 I. Rossetti, L. Sordelli, P. Ghigna, S. Pin, M. Scavini and L. Forni, *Inorg. Chem.*, 2011, **50**, 3757–3765.
30 A. Shih, C. Hor, D. Mueller, C.R.K. Marrian, W.T. Elam, P. Wolf, J.P. Kirkland and R.A. Neiser, *J. Vac. Sci. Tecnol. A*, 1988, **6**, 1058–1062.
31 H. S. Zeng, K. Inazu and K. Aika, *J. Catal.*, 2002, **211**, 33–41.

Table of Contents Entry